Int. J. Heat Mass Transfer. Vol. 30, No. 9, pp. 1871–1878, 1987
Printed in Great Britain

0017–9310/87 $3.00 + 0.00
Pergamon Journals Ltd.

Solution of the penetrating evaporation front model for finite porous medium using orthogonal collocation method

B. PALÁNCZ
Electrical Power Research Institute, Budapest, Hungary

(*Received* 22 *August* 1986)

Abstract—An orthogonal collocation solution of the penetrating evaporation front model for finite one-dimensional slab geometry is presented. Instead of using the moving boundary tracking technique, the transformation method proposed by Liapis and Litchfield was employed. Numerical experiments indicate that this procedure is more efficient than the finite difference method. Results given by this model are in good agreement with experimental findings.

INTRODUCTION

THE PENETRATING evaporation front model (PEFM), proposed originally in 1929, describing heat and mass transfer processes in capillary porous bodies during the falling drying rate period, has been studied, improved and verified experimentally by others, i.e. Luikov [1, 2] and Szentgyörgyi [3].

Unfortunately, it is not easy to solve the equations of this model and it needs considerable mathematical skill or too much computational effort.

For half-space geometry Gupta [4] published an approximate solution, and later Mikhailov [5] presented an analytical exact solution. For finite slab geometry Szentgyörgyi and Molnár [6] suggested a numerical procedure employing the moving boundary tracking technique (MBTT) combined with the finite difference method (FDM).

In this paper the orthogonal collocation technique (OCT) will be used to calculate temperature and moisture content distributions provided by PEFM. The reader can find detailed information on this numerical method in the excellent book by Finlayson [8]. The method itself has already been applied to the moving boundary problem concerning freeze drying by Liapis and Litchfield [9].

It can be shown that OCT is very efficient for solving the more complex PEFM problem too. This method opens the way for economical and practical engineering applications of this model.

PENETRATING EVAPORATION FRONT MODEL

During the falling drying rate period, when the moisture content falls down below a critical level, u_{cr}, the liquid transport is practically stopped. Consequently the phase change criterion, ε, jumps up to 1 discontinuously. A shock wave defined by the critical moisture content starts to penetrate into the wet material. If we suppose that behind this moving front the vaporization is so vigorous that no free liquid exists there, only bounded moisture content characterized by the equilibrium value, u_e, depending on the state of drying gas, we get the PEFM, see Fig. 1. This physical model proved to be more realistic than the original Luikov model, especially for modelling drying of granular substances.

The PEFM can be defined by the equations given below.

Region I

Because there is no liquid transport behind the evaporation front, the heat transport can be described as

$$\frac{\partial T_I}{\partial t} = a_I \frac{\partial^2 T_I}{\partial z^2}. \tag{1}$$

The vapour diffusion process has a very small time constant, therefore a quasi-steady state approach may be used

$$N_{wI} = \frac{D_I}{\xi}(p_{w\xi} - p_{ws}). \tag{2}$$

Region II

Here the original Luikov model can be considered, namely

$$\frac{\partial T_{II}}{\partial t} = a_{II} \frac{\partial^2 T_{II}}{\partial z^2} + a_m b \frac{\partial^2 u_{II}}{\partial z^2} \tag{3}$$

$$\frac{\partial u_{II}}{\partial t} = a_m \frac{\partial^2 u_{II}}{\partial z^2}. \tag{4}$$

The boundary conditions are given below.

(a) At $z = 0$

$$\alpha_c(T_g - T_s) = -\lambda_I \frac{\partial T_I}{\partial z} \tag{5}$$

NOMENCLATURE

a	diffusivity [$m^2 s^{-1}$]
$A_{ij}, \tilde{A}_{ij}$	elements of the collocation matrices A and $\tilde{A}$
b	$r\varepsilon/c_h$ [°C]
$B_{ij}, \tilde{B}_{ij}$	elements of the collocation matrices B and $\tilde{B}$
c_h	specific heat capacity [W s kg^{-1} °C^{-1}]
$d_i(t)$	functions in the temperature profiles [°C]
D_w	diffusion coefficient of vapour [$m^2 s^{-1}$]
$e_i(t)$	functions in the moisture content profiles
i	specific enthalpy [W s kg^{-1}]
L	thickness [m]
M	number of the inner collocation points in Region I
N	evaporation rate [kg $m^{-2} s^{-1}$]
p	pressure [N m^{-2}]
r	evaporation heat [W s kg^{-1}]
t	time [s]
T	temperature [°C or K]
$\tilde{T}$	$(T_g + T_{wb})/2$ [K]
u	moisture content [kg moisture/kg dry solid]
x	space coordinate [m].

Greek symbols

α_c	heat transfer coefficient [W m^{-2} °C^{-1}]
ε	phase change criterion
ξ_j	thickness of the jth finite element [m]
η, μ, ϕ, ψ	dimensionless space coordinates
ξ	position of the evaporation front [m]
λ	conductivity, mass [kg $m^{-1} s^{-1}$], heat [W m^{-1} °C^{-1}]
ρ_{st}	total density of solid [kg m^{-3}]
σ	evaporation coefficient [s m^{-1}]
v	wetting coefficient.

Subscripts

c	convective
cr	critical value
g	gas
h	thermal
l	liquid
m	mass
s	solid surface
w	vapour
wb	wet bulb
ξ	evaporation front
0	initial value
I, II	properties in Regions I and II, respectively.

$$\sigma(p_{ws} - p_{wg}) = \frac{D_I}{\xi}(p_{w\xi} - p_{ws}) \tag{6}$$

(b) At $z = \xi$. The mass balance for the evaporation front gives (see Fig. 2)

$$v\rho_{st}(u_I - u_{cr})\frac{d\xi}{dt} = \varepsilon\lambda_m \frac{\partial u_{II}}{\partial z} - N_{w\xi}. \tag{7}$$

Assuming that behind the front $u_I = u_e$, we get

$$N_{w\xi} = m\frac{d\xi}{dt} + \varepsilon\lambda_m \frac{\partial u_{II}}{\partial z} \tag{8}$$

where

$$m = v\rho_{st}(u_{cr} - u_e). \tag{9}$$

At the front the moisture content remains constant, namely

$$u_{II} = u_{cr}. \tag{10}$$

The partial vapour pressure can be computed from the tension curve relationship

$$\log p_{w\xi} = 2.7486 + \frac{7.5T_\xi}{238 + T_\xi}. \tag{11}$$

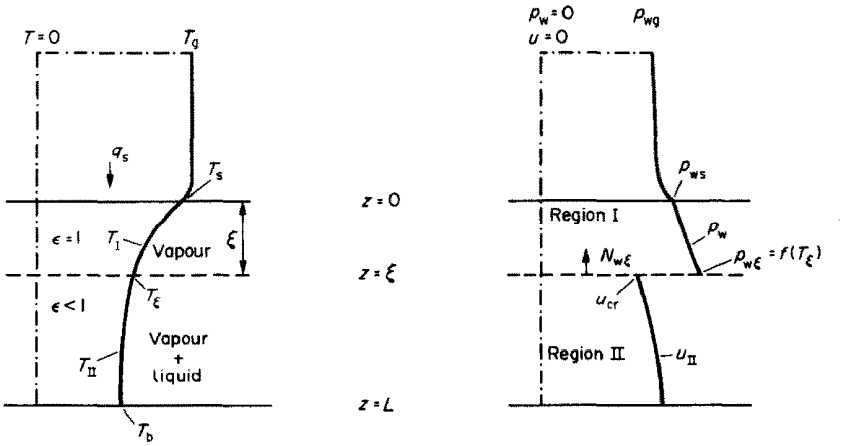

FIG. 1. Penetrating evaporation front model.

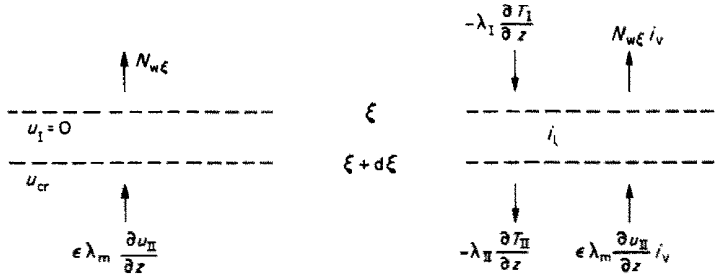

FIG. 2. Mass and heat balances for the moving front.

Because of the quasi-steady state approach for Region I

$$N_{w\xi} = N_{wI}. \tag{12}$$

The heat balance for the evaporation front yields (see Fig. 2)

$$v\rho_{st}(u_l - u_{cr})i_l \frac{d\xi}{dt} = \lambda_m \frac{\partial u_{II}}{\partial z} \varepsilon i_w - \lambda_l \frac{\partial T_I}{\partial z} - \left[N_{w\xi} i_w - \lambda_{II} \frac{\partial T_{II}}{\partial z} \right] \tag{13}$$

considering equation (8) and that

$$r = i_w - i_l \tag{14}$$

one may get

$$\left(N_{w\xi} - \varepsilon \lambda_m \frac{\partial u_{II}}{\partial z} \right) r = \lambda_{II} \frac{\partial T_{II}}{\partial z} - \lambda_I \frac{\partial T_I}{\partial z} \tag{15}$$

or

$$rm \frac{d\xi}{dt} = \lambda_{II} \frac{\partial t_{II}}{\partial z} - \lambda_l \frac{\partial T_I}{\partial z}. \tag{16}$$

(c) At $z = L$

$$\frac{\partial T_{II}}{\partial z} = \frac{\partial u_{II}}{\partial z} = 0. \tag{17}$$

Initial conditions for the evaporation front model

The falling drying rate period begins and the evaporation front starts to penetrate at $t = t_{cr}$, when

$$u(0, t_{cr}) = u_{cr}. \tag{18}$$

This equation defines the time point, from which the model is supposed to be valid. For $t < t_{cr}$, one may use the standard Luikov model [10]. Then at $t = t_{cr}$ we get

$$u_{II}(z, t_{cr}) = u(L - x, t_{cr}) \tag{19}$$

and

$$T_{II}(z, t_{cr}) = T(L - x, t_{cr}). \tag{20}$$

The velocity of the penetration front at $t = t_{cr}$, can be calculated by 'joining' the two models for $t = t_{cr}$. Then from equation (16) one can get at $x = L$

$$rm(\dot{\xi})_{t=t_{cr}} = \alpha_c(T_g - T_s) - \lambda_h \frac{\partial T}{\partial x}. \tag{21}$$

SOLUTION OF THE MODEL

In order to 'immobilize' the moving evaporation front, let us introduce two dimensionless space variables

$$\mu = \frac{z}{\xi}, \quad \phi = \frac{z - \xi}{L - \xi}, \quad 0 \leqslant \mu, \phi \leqslant 1. \tag{22}$$

Using the transformation proposed by Liapis and Litchfield [9], it can be written:

for equation (1)

$$\frac{\partial T_I}{\partial t} = \frac{\mu}{\xi} \frac{d\xi}{dt} \frac{\partial T_I}{\partial \mu} + \frac{a_l}{\xi^2} \frac{\partial^2 T_I}{\partial \mu^2}, \quad 0 < \mu < 1; \tag{23}$$

for equation (3)

$$\frac{\partial T_{II}}{\partial t} = \frac{1 - \phi}{L - \xi} \frac{d\xi}{dt} \frac{\partial T_{II}}{\partial \phi} + \frac{a_{II}}{(L - \xi)^2} \frac{\partial^2 T_{II}}{\partial \phi^2} + \frac{a_m b}{(L - \xi)^2} \frac{\partial^2 u_{II}}{\partial \phi^2}, \quad 0 < \phi < 1; \tag{24}$$

for equation (4)

$$\frac{\partial u_{II}}{\partial t} = \frac{1 - \phi}{L - \xi} \frac{d\xi}{dt} \frac{\partial u_{II}}{\partial \phi} + \frac{a_m}{(L - \xi)^2} \times \frac{\partial^2 u_{II}}{\partial \phi^2}, \quad 0 < \phi < 1; \tag{25}$$

for equation (8)

$$N_{w\xi} = m \frac{d\xi}{dt} + \frac{\varepsilon \lambda_m}{L - \xi} \frac{\partial u_{II}}{\partial \phi}, \quad \phi = 0; \tag{26}$$

for equation (5)

$$\alpha_c(T_g - T_s) = -\frac{\lambda_l}{\xi} \frac{\partial T_I}{\partial \mu}, \quad \mu = 0; \tag{27}$$

for equation (16)

$$rm \frac{d\xi}{dt} = \frac{\lambda_{II}}{L - \xi} \frac{\partial T_{II}}{\partial \phi} - \frac{\lambda_I}{\xi} \frac{\partial T_I}{\partial \mu}, \quad \mu = 1 \quad \text{and} \quad \phi = 0. \tag{28}$$

In order to apply orthogonal collocation, let us introduce

$$\psi = 1-\phi \quad \text{and} \quad \eta = 1-\mu. \tag{29}$$

The temperature and moisture content distribution can then be approximated by the following polynomial functions:

Region I

$$T_{\mathrm{I}}(\eta, t) = \sum_{j=1}^{M+2} d_{\mathrm{I},j}(t)\eta^{j-1}, \quad 0 \leqslant \eta \leqslant 1; \tag{30}$$

Region II

$$T_{\mathrm{II}}(\psi, t) = \sum_{i=1}^{N+1} d_{\mathrm{II},i}(t)\psi^{2(i-1)} \tag{31}$$

$$u_{\mathrm{II}}(\psi, t) = \sum_{i=1}^{N+1} e_{\mathrm{II},i}(t)\psi^{2(i-1)}, \tag{32}$$

$$0 \leqslant \psi \leqslant 1.$$

Our collocation equations are now:

Region I: at $\eta = \eta_j, j = 2, 3, \ldots, M+1$

$$\frac{\mathrm{d}T_{\mathrm{I},j}}{\mathrm{d}t} = -\frac{1-\eta_j}{\xi}\frac{\mathrm{d}\xi}{\mathrm{d}t}\sum_{k=1}^{M+2}\tilde{A}_{jk}T_{\mathrm{I},k} + \frac{a_{\mathrm{I}}}{\xi^2}\sum_{k=1}^{M+2}\tilde{B}_{jk}T_{\mathrm{I},k} \tag{33}$$

where

$$T_{\mathrm{I},1} = T_\xi \quad \text{and} \quad T_{\mathrm{I},M+2} = T_{\mathrm{s}}; \tag{34}$$

Region II: at $\psi = \psi_i, i = 1, 2, \ldots, N$

$$\frac{\mathrm{d}u_{\mathrm{II},i}}{\mathrm{d}t} = -\frac{\psi_i}{L-\xi}\frac{\mathrm{d}\xi}{\mathrm{d}t}\sum_{k=1}^{N+1}A_{ik}u_{\mathrm{II},k} + \frac{a_{\mathrm{m}}}{(L-\xi)^2}\sum_{k=1}^{N+1}B_{ik}u_{\mathrm{II},k} \tag{35}$$

$$\frac{\mathrm{d}T_{\mathrm{II},i}}{\mathrm{d}t} = -\frac{\psi_i}{L-\xi}\frac{\mathrm{d}\xi}{\mathrm{d}t}\sum_{k=1}^{N+1}A_{ik}T_{\mathrm{II},k} + \frac{a_{\mathrm{II}}}{(L-\xi)^2} \times \sum_{k=1}^{N+1}B_{ik}T_{\mathrm{II},k} + \frac{a_{\mathrm{m}}b}{(L-\xi)^2}\sum_{k=1}^{N+1}B_{ik}u_{\mathrm{II},k} \tag{36}$$

where

$$T_{\mathrm{II},N+1} = T_\xi \quad \text{and} \quad u_{\mathrm{II},N+1} = u_{\mathrm{cr}}. \tag{37}$$

Boundaries

at $\eta = 1, j = M+2$

$$\alpha_{\mathrm{c}}(T_{\mathrm{g}} - T_{\mathrm{s}}) = \frac{\lambda_{\mathrm{I}}}{\xi}\sum_{k=1}^{M+2}\tilde{A}_{M+2,k}T_{\mathrm{I},k} \tag{38}$$

at $\psi = 1, i = N+1$

$$N_{\mathrm{w}\xi} = m\frac{\mathrm{d}\xi}{\mathrm{d}t} - \frac{\varepsilon\lambda_{\mathrm{m}}}{L-\xi}\sum_{k=1}^{N+1}A_{N+1,k}u_{\mathrm{II},k} \tag{39}$$

at $\psi = 1$ and $\eta = 0; i = N+1, j = 1$

$$rm\frac{\mathrm{d}\xi}{\mathrm{d}t} = -\frac{\lambda_{\mathrm{II}}}{L-\xi}\sum_{k=1}^{N+2}A_{N+1,k}T_{\mathrm{II},k} + \frac{\lambda_{\mathrm{I}}}{\xi}\sum_{k=1}^{M+2}\tilde{A}_{1,k}T_{\mathrm{I},k}. \tag{40}$$

We now have $2N+M+1$ differential equations, equations (33), (35), (36) and (40), as well as five algebraic ones, equations (2), (6), (11), (38) and (39). The unknown variables are: $T_{\mathrm{I},j}$, $j = 2, \ldots, M+1$; $T_{\mathrm{II},i}$ and $u_{\mathrm{II},i}$, $i = 1, 2, \ldots, N$; ξ, T_{s}, T_ξ, $p_{\mathrm{w}\xi}$, p_{ws} and $N_{\mathrm{w}\xi}$.

Equation (11) is nonlinear, therefore the following iteration procedure may be used to solve the algebraic equations:

(a) guess T_ξ;
(b) compute $p_{\mathrm{w}\xi}$ from equation (11);
(c) compute p_{ws} from equation (6)

$$p_{\mathrm{ws}} = \frac{\sigma p_{\mathrm{wg}}\xi + D_{\mathrm{I}}p_{\mathrm{w}\xi}}{\sigma\xi + D_{\mathrm{I}}}; \tag{41}$$

(d) considering equations (2), (6) and (12), compute $N_{\mathrm{w}\xi}$

$$N_{\mathrm{w}\xi} = \sigma(p_{\mathrm{ws}} - p_{\mathrm{wg}}); \tag{42}$$

(e) compute $\dot{\xi}$ from equation (39)

$$\frac{\mathrm{d}\xi}{\mathrm{d}t} = \frac{1}{m}\left[N_{\mathrm{w}\xi} + \frac{\varepsilon\lambda_{\mathrm{m}}}{L-\xi}\sum_{k=1}^{N+1}A_{N+1,k}u_{\mathrm{II},k}\right]; \tag{43}$$

(f) compute T_{s} from equation (38)

$$T_{\mathrm{s}} = \frac{\alpha_{\mathrm{c}}T_{\mathrm{g}} - \frac{\lambda_{\mathrm{I}}}{\xi}\sum_{k=1}^{M+1}\tilde{A}_{M+2,k}T_{\mathrm{I},k}}{\alpha_{\mathrm{c}} + \tilde{A}_{M+2,M+2}\frac{\lambda_{\mathrm{I}}}{\xi}}; \tag{44}$$

(g) our guess for T_ξ can be checked by equation (40)

$$T_\xi = \left(rm\frac{\mathrm{d}\xi}{\mathrm{d}t} + \frac{\lambda_{\mathrm{II}}}{L-\xi}\sum_{k=1}^{N}A_{N+1,k}T_{\mathrm{II},k} - \frac{\lambda_{\mathrm{I}}}{\xi}\sum_{k=2}^{M+2}\tilde{A}_{1,k}T_{\mathrm{I},k}\right)\Big/\left(\frac{\lambda_{\mathrm{I}}}{\xi}\tilde{A}_{11} - \frac{\lambda_{\mathrm{II}}}{L-\xi}A_{N+1,N+1}\right). \tag{45}$$

At $t = t_{\mathrm{cr}}$, we can compute $(\dot{\xi})_{t=t_{\mathrm{cr}}}$ from equation (21), which is in collocation form

$$rm(\dot{\xi})_{t=t_{\mathrm{cr}}} = \alpha_{\mathrm{c}}(T_{\mathrm{g}} - T_{\mathrm{s}}) - \frac{\lambda_{\mathrm{h}}}{L}\sum_{i=1}^{N+1}A_{N+1,i}T_i. \tag{46}$$

To start the computation with the penetrating front model, we have to calculate a penetration distance ξ_0, which belongs to $(\dot{\xi})_{t=t_{\mathrm{cr}}}$ and defined by equations (41)–(45).

NUMERICAL STUDY

Let us illustrate the application of this modelling and simulation procedure by the following example.

The numerical data for the calculation are given in Table 1.

Now, let us employ the one-point collocation in both regions, $M = N = 1$. The profiles are approximated by the following second-order polynomial

Table 1. Data used for numerical calculation

$T_g = 45°C$	$a_m = 2.633 \times 10^{-8}\ m^2\ s^{-1}$	$\rho_{st} = 900\ kg\ m^{-3}$
$p_{wg} = 1538.37\ N\ m^{-2}$	$a_h = 3.292 \times 10^{-7}\ m^2\ s^{-1}$	$D_I = D_w/(R_w\tilde{T}) = 4.1675 \times 10^{-10}\ s$
$r = 2.382 \times 10^6\ W\ s\ kg^{-1}$	$\lambda_h = 0.93\ W\ m^{-1}\ °C^{-1}$	$\lambda_I = 0.73\ W\ m^{-1}\ °C^{-1}$
$c_h = 1980\ W\ s\ kg^{-1}\ °C^{-1}$	$\lambda_m = 3.95 \times 10^{-5}\ kg\ m^{-1}\ s^{-1}$	$a_I = 2.361 \times 10^{-7}\ m^2\ s^{-1}$
$\alpha_c = 10.5\ W\ m^{-2}\ °C^{-1}$	$u_{cr} = 0.2$ kg moisture/kg dry solid	$\lambda_{II} = \lambda_h$
$\sigma = 6.2637 \times 10^{-8}\ s\ m^{-1}$	$k_1 = -244$	$a_{II} = a_h$
$\varepsilon = 0.1$	$k_2 = -11.2$	$\nu = 1$
$L = 0.045$ m		

functions:

$$T_I(\eta, t) = d_{I,1}(t) + d_{I,2}(t)\eta + d_{I,3}(t)\eta^2, \quad 0 \leqslant \eta \leqslant 1 \quad (47)$$

$$T_{II}(\psi, t) = d_{II,1}(t) + d_{II,2}(t)\psi^2$$

$$u_{II}(\psi, t) = e_{II,1}(t) + e_{II,2}(t)\psi^2, \quad 0 \leqslant \psi \leqslant 1. \quad (48)$$

The collocation points can be seen on Fig. 3. The collocation equations are:

at $\eta_2 = 0.5$

$$\frac{dT_{I,2}}{dt} = -\frac{1}{2\xi}\frac{d\xi}{dt}(\tilde{A}_{21}T_\xi + \tilde{A}_{22}T_{I,2} + \tilde{A}_{23}T_s) + \frac{a_I}{\xi^2}(\tilde{B}_{21}T_\xi + \tilde{B}_{22}T_{I,2} + \tilde{B}_{23}T_s); \quad (49)$$

at $\psi_1 = 0.4472$

$$\frac{dT_{II,2}}{dt} = -\frac{0.4472}{L-\xi}\frac{d\xi}{dt}(A_{11}T_{II,1} + A_{12}T_\xi) + \frac{a_{II}}{(L-\xi)^2}(B_{11}T_{II,1} + B_{12}T_\xi) + \frac{a_m b}{(L-\xi)^2}(B_{11}u_{II,1} + B_{12}u_{cr}) \quad (50)$$

$$\frac{du_{II,1}}{dt} = -\frac{0.4472}{L-\xi}\frac{d\xi}{dt}(A_{11}u_{II,1} + A_{12}u_{cr}) + \frac{a_m}{(L-\xi)^2}(B_{11}u_{II,1} + B_{12}u_{cr}). \quad (51)$$

Now, equations (43)–(45) have the following form:

$$\frac{d\xi}{dt} = \frac{1}{m}\left[N_{w\xi} + \frac{\varepsilon\lambda_m}{L-\xi}(A_{11}u_{II,1} + A_{12}u_{cr})\right] \quad (52)$$

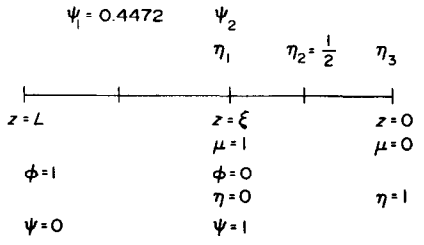

FIG. 3. Location of the collocation points in different coordinate systems.

$$T_s = \frac{\alpha_c T_g - \frac{\lambda_I}{\xi}(\tilde{A}_{31}T_\xi + \tilde{A}_{32}T_{I,2})}{\alpha_c + \frac{\lambda_I}{\xi}\tilde{A}_{33}} \quad (53)$$

and

$$T_\xi = \left(rm\frac{d\xi}{dt} + \frac{\lambda_{II}}{L-\xi}A_{21}T_{II,1} - \frac{\lambda_I}{\xi}(\tilde{A}_{12}T_{I,1} + \tilde{A}_{13}T_s)\right) \Big/ \left(\frac{\lambda_I}{\xi}\tilde{A}_{11} - \frac{\lambda_{II}}{L-\xi}A_{22}\right). \quad (54)$$

At $t = t_{cr}$, we may use the linear approximation to find $T_{I,1}(t_{cr})$, namely

$$T_{I,1}(t_{cr}) = (T_s + T_\xi)/2. \quad (55)$$

Matrices A and $\tilde{A}$ are given in Table 2.

In Region I the temperature profile can be calculated as

$$T_I(\eta, t) = T_\xi(t) + [4T_{I,2}(t) - 3T_\xi(t) - T_s(t)]\eta + [2T_s(t) - 4T_{I,2}(t) + 2T_\xi(t)]\eta^2, \quad M = 1 \quad (56)$$

where the coefficients $d_{I,i}(t)$, $i = 1, 2, \ldots, M+2$ are determined by the equation system

$$T_{I,j}(t) = T_I(\eta_j, t) = \sum_{i=1}^{M+2} d_{I,i}(t)\eta_j^{i-1}, \quad j = 1, 2, \ldots, M+2. \quad (57)$$

Computations were carried out with the standard Luikov model [10] until $u_s(t) = u_{cr} = 0.2$. Then the penetrating evaporation front model was used. The results of these computations can be seen on Figs. 4–9.

Table 2. Coefficients of collocation matrices [8]

For Region I:

$$\tilde{A} = \begin{pmatrix} -3 & 4 & -1 \\ -1 & 0 & 1 \\ 1 & -4 & 3 \end{pmatrix}, \quad \tilde{B} = \begin{pmatrix} 4 & -8 & 4 \\ 4 & -8 & 4 \\ 4 & -8 & 4 \end{pmatrix}$$

For Region II:

$$A = \begin{pmatrix} -1.118 & 1.118 \\ -2.500 & 2.500 \end{pmatrix}, \quad B = \begin{pmatrix} -2.500 & 2.500 \\ -2.500 & 2.500 \end{pmatrix}$$

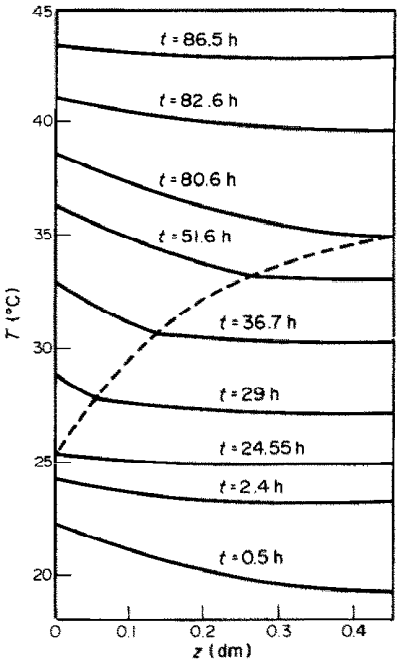

FIG. 4. Temperature distribution.

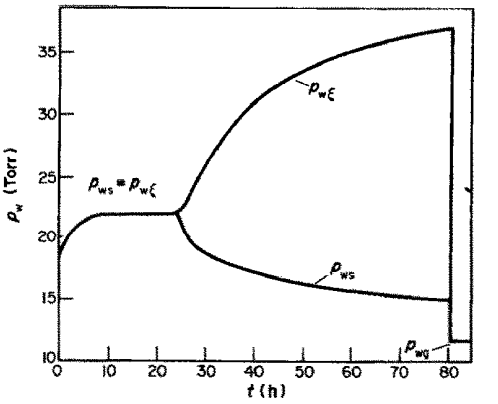

FIG. 6. Vapour partial pressure history at the solid surface and at the moving front during the drying process.

Figures 7 and 8 show close similarities to the solution obtained for the half-space geometry [4, 5].

Figure 9 shows, that the sorption isotherm model [7], estimates of higher evaporation rate than the evaporation front model and therefore somewhat lower wet material temperature. The main difference between the two models is in the predicted moisture content profiles. Figure 10 compared with Fig. 7 in ref. [11] indicates very good qualitative agreement

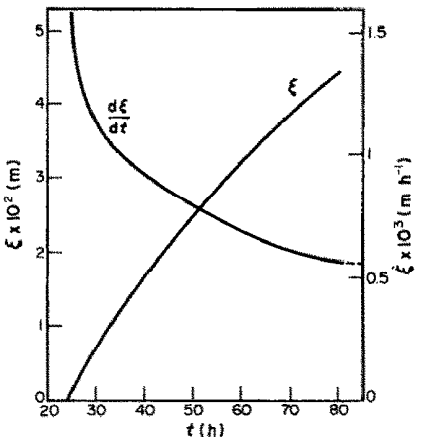

FIG. 7. Position and velocity of the moving evaporation front vs time.

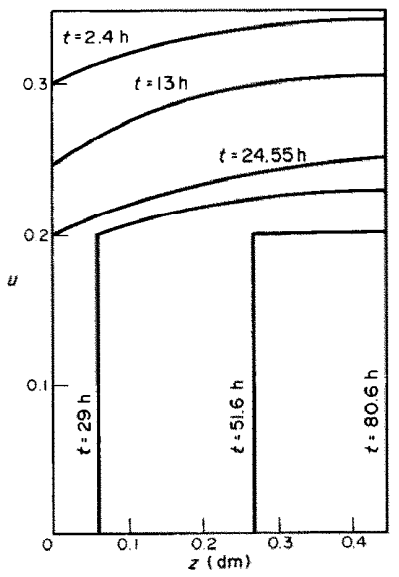

FIG. 5. Moisture content distribution.

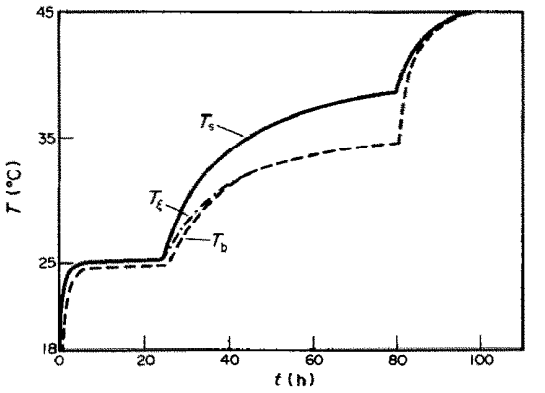

FIG. 8. Temperature history at the solid surface, ——; and at the bottom of the slab, – – –; and at the moving front, · · ·

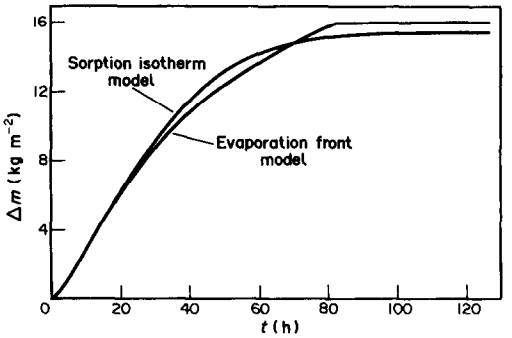

FIG. 9. Total evaporated moisture from 1 m² solid surface vs drying time, computed on the basis of the two different models.

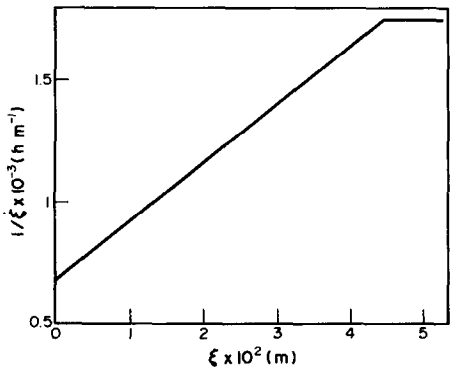

FIG. 10. Reciprocal values of the velocity of front movement vs front depth.

between the results of the PEFM and experimental findings [11].

CONCLUSIONS

A penetrating evaporation front model was developed and solved for finite slab geometry. The orthogonal collocation technique provided a very simple and practical method to solve the model equations. Consequently, one does not need to employ unnecessary physical or geometrical simplifications, or special mathematical skill to solve the drying problem in the falling rate period.

Comparing numerical results and experimental findings, even a few collocation points proved to be satisfactory for giving a good approximation.

The method can be easily adapted to other geometries too [12].

Acknowledgements—The author would like to thank Prof. Dr S. Endrényi for his many suggestions which have resulted in significant improvements in the paper.

REFERENCES

1. A. V. Luikov, *Heat and Mass Transfer in Capillary Porous Bodies*. Pergamon Press, Oxford (1966).
2. A. V. Luikov, System of differential equations of heat and mass transfer in capillary porous bodies, *Int. J. Heat Mass Transfer* **18**, 1–17 (1975).
3. S. Szentgyörgyi, Drying of capillary porous materials in the second falling-rate periods, *Proc. of the Third Int. Symp. on Drying*, Birmingham, pp. 100–109 (1982).
4. L. N. Gupta, An approximate solution of the generalized Stefan's problem in a porous medium, *Int. J. Heat Mass Transfer* **17**, 313 (1974).
5. M. D. Mikhailov, Exact solution of temperature and moisture distributions in a porous half-space with moving evaporation front, *Int. J. Heat Mass Transfer* **18**, 797 (1975).
6. S. Szentgyörgyi and K. Molnár, Drying of macroporous systems, *Periodica Polytech., Mech. Engng, Budapest* **20**, 47–65 and 97–115 (1976).
7. M. Parti and B. Paláncz, Mathematical models for batch drying, *Int. J. Heat Mass Transfer* **17**, 669 (1974).
8. B. A. Finlayson, *Nonlinear Analysis in Chemical Engineering*. McGraw-Hill, New York (1980).
9. A. I. Liapis and R. J. Litchfield, Numerical solution of moving boundary transport problems in finite media by orthogonal collocation, *Comput. Chem. Engng* **3**, 615 (1979).
10. B. Paláncz, Simulation of heat and mass transfer in a finite porous medium using orthogonal collocation method, *Wärme- und Stoffübertragung* **19**, 229 (1985).
11. S. Szentgyörgyi and M. Örvös, An approximation method for the determination of the distribution of temperature and of moisture content in the falling rate period of drying, *Drying Technol.* **3**, 399 (1985).
12. B. Paláncz, Modelling and simulation of heat and mass transfer in a packed bed of solid particles having high diffusion resistance, *Comput. Chem. Engng* **6**, 567 (1985).

SOLUTION DU MODELE DE FRONT D'EVAPORATION MOBILE DANS UN MILIEU POREUX FINI PAR UNE METHODE DE COLLOCATION ORTHOGONALE

Résumé—On présente une méthode de collocation orthogonale pour traiter le modèle de front d'évaporation pénétrant dans une géométrie monodimensionnelle de couche. Au lieu d'utiliser la technique de frontière mobile, on a recours à la méthode de transformation proposée par Liapis et Litchfield. Des essais numériques montrent que cette procédure est plus efficace que la méthode aux différences finies. Les résultats donnés par ce modèle sont en bon accord avec les données expérimentales.

EIN MODELL MIT WANDERNDER VERDAMPFUNGSFRONT IN ENDLICHEN PORÖSEN KÖRPERN—LÖSUNG MIT DER ORTHOGONALEN KOLLOKATIONS-METHODE

Zusammenfassung—Es wird eine orthogonale Kollokationslösung des Modells der wandernden Verdampfungsfront in einer begrenzten eindimensionalen Scheibe vorgestellt. Anstatt die Abgleichmethode für bewegte Berandungen zu benutzen, wurde die von Liapis und Litchfield vorgestellte Transformationsmethode benutzt. Numerische Experimente zeigen, daß diese Vorgehensweise aussichtsreicher ist als die Finite-Differenzen-Methode. Ergebnisse aufgrund dieses Modells stimmen gut mit experimentellen Daten überein.

ОПРЕДЕЛЕНИЕ ДВИЖЕНИЯ ФРОНТА ИСПАРЕНИЯ ДЛЯ КОНЕЧНОЙ ПОРИСТОЙ СРЕДЫ С ПОМОЩЬЮ МЕТОДА ОРТОГОНАЛЬНЫХ КОЛЛОКАЦИЙ

Аннотация—Методом ортогональных коллокаций получено решение задачи о движущемся фронте испарения для плоской пористой пластины. При решении использовался метод, предложенный Лайаписом и Литчфилдом. Численные эксперименты показали, что предложенная методика более эффективна, чем метод конечных разностей. Результаты, полученные с помощью этой модели, хорошо согласуются с экспериментальными данными.